Pergamon

Int. J. Heat Mass Transfer. Vol. 40, No. 6, pp. 1261–1277, 1997

0017-9310/97 $17.00 + 0.00

PII: S0017-9310(96)00182-2

The effects of longitudinal heat conduction in compact plate-fin and tube-fin heat exchangers using a finite element method

Ch. RANGANAYAKULU
Aircraft Design Bureau, L.C.A. Complex, Hindustan Aeronautics Limited, Bangalore 560 037, India

K. N. SEETHARAMU
Department of Mechanical Engineering, Indian Institute of Technology, Madras 600 036, India

and

K. V. SREEVATSAN
Aircraft Design Bureau, L.C.A. Complex, Hindustan Aeronautics Limited, Bangalore 560 037, India

(*Received for publication* 18 *June* 1996)

Abstract—An analysis of the crossflow plate-fin, crossflow tube-fin, counterflow plate-fin and parallel flow plate-fin compact heat exchangers accounting for the effect of 'longitudinal heat conduction' through the exchanger wall is carried out using a finite element method. The exchanger effectiveness and its deterioration due to the longitudinal heat conduction effect have been calculated for various designs and operating conditions of the exchanger. The results indicate that the thermal performance deterioration of crossflow plate-fin, crossflow tube-fin and counterflow plate-fin heat exchangers due to longitudinal heat conduction may become significant especially when the fluid capacity rate ratio is equal to one and when the longitudinal heat conduction parameter is large. Copyright © 1996 Elsevier Science Ltd.

INTRODUCTION

The demand for high performance heat exchange devices having small spacial dimensions is increasing due to their requirement in applications such as aerospace and automobile vehicles, cooling of electronic equipment and artificial organs [1]. The accurate prediction of the thermal performance of a compact heat exchanger in the design stage is highly desirable for most aerospace applications. The design theory of compact heat exchangers is based on either the ε-NTU or the log-mean temperature difference concept. In a heat exchanger, since heat transfer takes place, temperature gradients exist in both fluids and in the separating wall, in the fluid flow directions. In the theory described earlier, the longitudinal heat conduction (LHC) effect in fluids and in the wall were neglected in deriving exchanger ε-NTU expressions [2]. The advancement of heat exchanger design theory, which takes these effects into consideration, therefore becomes an important project in industry. Also, constant thermophysical property assumptions leading to a constant heat transfer coefficient are used in heat exchanger design. There is a need to develop a method which takes into account the variable fluid property effect along with LHC effects in the heat exchangers.

In this paper, the effects of LHC using a finite element method are presented and discussed for crossflow plate-fin, crossflow tube-fin, counterflow plate-fin and parallel-flow plate-fin compact heat exchangers. The LHC through the heat exchanger wall structure in the direction of the fluid flow has the effect of decreasing the exchanger performance for a specified NTU, and this reduction may be quite serious in exchangers with a short flow length designed for high effectiveness ($\varepsilon > 80\%$) [3]. These effects have been well characterized and the numerical data are available in refs. [3–6] for periodic-flow heat exchangers.

Investigations of this effect for the direct transfer type heat exchangers (crossflow, counterflow and parallel-flow type) are limited [7–9]. All of them have neglected the effect of fluid and material property variations while investigating the LHC effects. Kroeger [9] stated that in most such cases, results obtained at an average material temperature matched closely with results from a detailed computer program, using fine nodal divisions and considering material property variations. However, Ravikumar *et al.* [10, 11] have developed a numerical procedure based on the finite element method to analyse the performance of crossflow plate-fin compact heat exchangers without considering the LHC effects. The present analysis has been carried out to determine the effects of LHC on

NOMENCLATURE

A	total heat transfer area [m^2]
a	elemental heat transfer area [m^2]
a'	elemental heat transfer area per unit core area, dimensionless
A_w	total solid elemental area available for longitudinal heat conduction [m^2]
c_p	specific heat of the fluid at constant pressure [J kg^{-1} K^{-1}]
C	Mc_p = fluid heat capacity rate [J s^{-2} K^{-1}]
h	convection heat transfer coefficient [W m^{-2} K^{-1}]
k	thermal conductivity of the exchanger wall [W m^{-1} K^{-1}]
L, l	the length of the elemental exchanger in x- or y-directions, respectively [m]
LHC	longitudinal heat conduction
M	mass flow rate [kg s^{-1}]
NTU	AU/C_{min} = number of transfer units, dimensionless
P	crossflow tube-fin exchanger tube perimeter [m]
Q	enthalpy/heat entering or leaving the plate [W]
q	enthalpy/heat entering/leaving the plate per unit area [W m^{-2}]
T	temperature of hot/cold fluids and metal wall [°C]
U	overall heat transfer coefficient [W m^{-2} K^{-1}]
VTHC	variable heat transfer coefficient case
x	flow length along hot fluid [m]
y	flow length along cold fluid [m].

Greek symbols

ε	exchanger effectiveness $= C_h(T_{h,in}-T_{h,o})/C_{min}(T_{h,in}-T_{c,in})$ $= C_c(T_{c,o}-T_{c,in})/C_{min}(T_{h,in}-T_{c,in})$
τ	conduction effect factor as defined in equation (24), dimensionless
λ	longitudinal heat conduction parameter as defined in equations (22) and (23), dimensionless
ϑ	overall surface efficiency, dimensionless.

Subscripts

c	cold side
b	bottom plate
h	hot side
in	inlet
m	middle plate
max	maximum magnitude
min	minimum magnitude
o	outlet
t	top plate
w	metal wall 1–16 node numbers when used with T or Q.

crossflow plate-fin, crossflow tube-fin, counterflow plate-fin and parallel-flow plate-fin heat exchangers. It has been observed that no study has been reported yet on the LHC problem for crossflow tube-fin and parallel-flow heat exchangers of either storage or direct transfer types.

FINITE ELEMENT METHOD

A discretized model of a crossflow plate-fin heat exchanger is shown in Fig. 1(a). It is divided into a number of equal strips. Strip 1 is isolated and shown in Fig. 1(b). The subject exchanger may be visualized as a wall, separating the two fluid streams flowing at right angles, with plate-fins on both sides, as shown in Fig. 1(c). Each strip consists of a number of pairs of 16-noded stacks which carry hot and cold fluids as shown in Fig. 1(d). Similarly, element stacks (10-noded) for a parallel-flow heat exchanger and a counterflow heat exchanger are shown in Fig. 1(e) and (f), respectively.

In the crossflow heat exchanger, a four-noded element has been considered for studying the two-dimensional LHC effects on exchanger wall. Since the heat transfer in counterflow and parallel-flow heat exchanger plates is merely one-dimensional, a two-noded element has been considered for LHC effects on the exchanger wall. Since the wall temperature distribution in a crossflow tube-fin heat exchanger is one-dimensional, a two-noded element has been considered for LHC effects in the exchanger tube as shown in Fig. 1 (g) and (h). These are the basic elemental exchangers for which the finite element equations are formulated as coupled conduction–convection problems [12] using Galerkin's method [13]. The linear elements (two-noded) for both hot and cold fluids are considered in the present analysis. The following assumptions are made in this analysis:

(1) The thickness of the exchanger wall is small when compared with its other two dimensions, so that the thermal resistance through the exchanger wall in the directional normal to the fluid flows is small enough to be neglected.
(2) There is no phase change and no heat generation within the exchanger.
(3) Fluids other than liquid metals are considered. Their temperatures remain constant and uniform over their respective inlet sections.

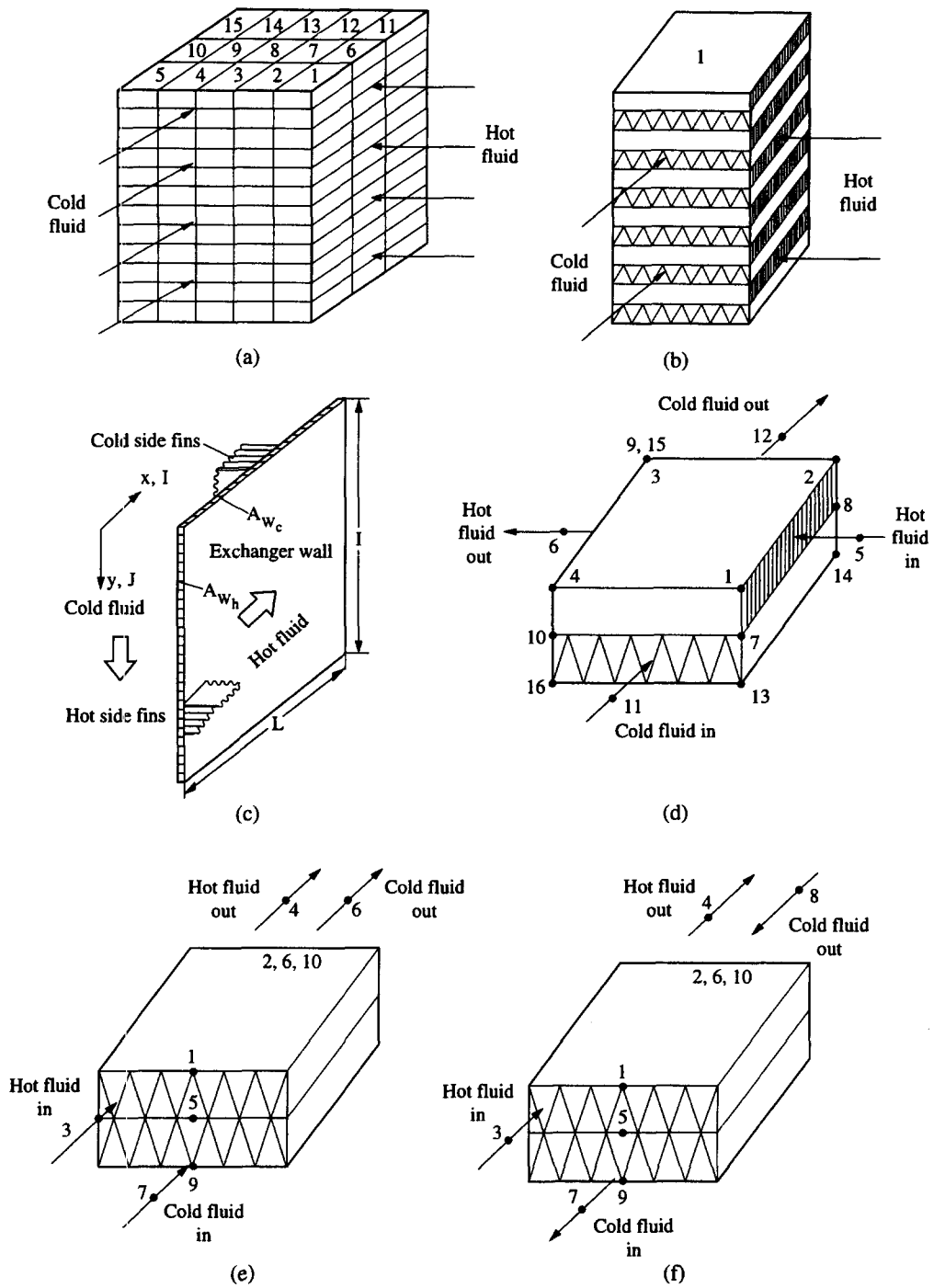

Fig. 1. Compact heat exchangers: (a) a discretised exchanger (crossflow plate-fin); (b) a strip 1 (crossflow plate-fin); (c) exchanger wall with fins; (d) an element stack (crossflow plate-fin); (e) an element stack (parallel-flow plate-fin); (f) an element stack (counterflow plate-fin); (g) tube-fin heat exchanger; (h) an element (tube-fin). (*Continued overleaf.*)

(4) The exchanger where both the fluids are unmixed is considered. Cross or transverse mixing of fluids is not considered.
(5) The heat transfer surface configurations and the heat transfer areas on both sides per unit base area are constant and uniform throughout the exchanger.
(6) In the elements, the temperatures of the fluid are assumed to vary only along their flow lengths.
(7) The entry length effects are not considered in the present analysis.
(8) Constant thermal conductivity is assumed for plate and fin metals.

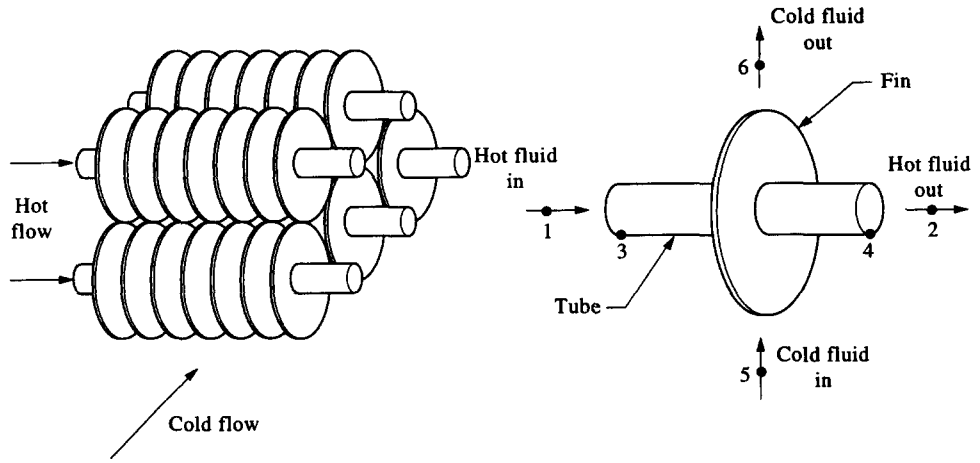

(g) (h)

Fig. 1—*continued.*

(9) Steady-state conditions are assumed.

Based on the above assumptions, the governing energy balance equations considering 2-D LHC on the exchanger plate and boundary conditions for a crossflow heat exchanger are formulated as shown below:

$$\frac{(kA_w)_h}{l}\frac{\partial^2 T_{w,t}}{\partial x^2}+\frac{(kA_w)_c}{L}\frac{\partial^2 T_{w,t}}{\partial y^2}-(\vartheta ha')_h(T_h-T_{w,t})=q_t \quad (1)$$

(for top plate)

$$-\frac{(MC_p)_h}{l}\frac{\partial T_h}{\partial x}+(\vartheta ha')_h(T_h-T_{w,t})+(\vartheta ha')_h(T_h-T_{w,m})=0 \quad (2)$$

(for hot fluid)

$$\frac{(kA_w)_h}{l}\frac{\partial^2 T_{w,m}}{\partial x^2}+\frac{(kA_w)_c}{L}\frac{\partial^2 T_{w,m}}{\partial y^2}-(\vartheta ha')_h(T_h-T_{w,m})+(\vartheta ha')_c(T_{w,m}-T_c)=0 \quad (3)$$

(for middle plate)

$$+\frac{(MC_p)_c}{L}\frac{\partial T_c}{\partial y}+(\vartheta ha')_c(T_{w,m}-T_c)+(\vartheta ha')_c(T_{w,b}-T_c)=0 \quad (4)$$

(for cold fluid)

$$\frac{(kA_w)_h}{l}\frac{\partial^2 T_{w,b}}{\partial x^2}+\frac{(kA_w)_c}{L}\frac{\partial^2 T_{w,b}}{\partial y^2}+(\vartheta ha')_c(T_{w,b}-T_c)=q_b \quad (5)$$

(for bottom plate)

and the boundary conditions are:

$$T_h(0,y)=T_{h,in} \quad T_c(x,0)=T_{c,in} \quad (6)$$

$$\frac{dT_w(0,y)}{dx}=\frac{dT_w(L,y)}{dx}=0$$

$$\frac{dT_w(x,0)}{dy}=\frac{dT_w(x,1)}{dy}=0. \quad (7)$$

Similarly, based on the above assumptions, the governing energy balance equations considering one-dimensional LHC in the counterflow and parallel-flow plate-fin exchangers, are given below:

$$\frac{(kA_w)_h}{L}\frac{\partial^2 T_{w,t}}{\partial x^2}-(\vartheta ha')_h(T_h-T_{w,t})=q_t \quad (8)$$

(for top plate)

$$-\frac{(MC_p)_h}{L}\frac{\partial T_h}{\partial x}+(\vartheta ha')_h(T_h-T_{w,t})+(\vartheta ha')_h(T_h-T_{w,m})=0 \quad (9)$$

(for hot fluid)

$$\frac{(kA_w)_h}{L}\frac{\partial^2 T_{w,m}}{\partial x^2}-(\vartheta ha')_h(T_h-T_{w,m})+(\vartheta ha')_c(T_{w,m}-T_c)=0 \quad (10)$$

(for middle plate)

$$+\frac{(MC_p)_c}{L}\frac{\partial T_c}{\partial x}+(\vartheta ha')_c(T_{w,m}-T_c)+(\vartheta ha')_c(T_{w,b}-T_c)=0 \quad (11)$$

(for cold fluid)

$$\frac{(kA_w)_h}{L}\frac{\partial^2 T_{w,b}}{\partial x^2}+(\vartheta ha')_c(T_{w,b}-T_c)=q_b \quad (12)$$

(for bottom plate).

Also, the governing energy balance equations considering the one-dimensional LHC in crossflow tube-

fin heat exchanger, are given below:

$$-(MC_p)_h\frac{\partial T_h}{\partial x}+(\vartheta hP)_h(T_h-T_w)=0 \quad (13)$$

(for hot fluid)

$$(kA_w)\frac{\partial^2 T_w}{\partial x^2}+(\vartheta hP)_h(T_h-T_w)$$

$$-(\vartheta hP)_c(T_w-T_c)=0 \quad (14)$$

(for tube)

$$(MC_p)_c\frac{\partial T_c}{\partial x}-(\vartheta hP)_c(T_w-T_c)=0 \quad (15)$$

(for cold fluid)

and the boundary conditions are:

$$T_h(0,y)=T_{h,in} \quad T_c(x,0)=T_{c,in} \quad (16)$$

$$\frac{dT_w(x,0)}{dy}=\frac{dT_w(x,1)}{dy}=0. \quad (17)$$

The temperature variations of the cold (T_c), hot (T_h) fluids, counterflow or parallel-flow heat exchanger plate (T_w) and crossflow heat exchanger tube (T_w) in the element are approximated by a linear variation as,

$$T_h=N_iT_i+N_jT_j \quad (18)$$

$$T_c=N_iT_i+N_jT_j \quad (19)$$

$$T_w=N_iT_i+N_jT_j \quad (20)$$

where N_i, N_j and T_i, T_j are the shape functions and temperatures, respectively, for the nodes i and j, where $N_i=1-x/L$, $N_j=x/L$, in which L is the element length. Similarly, the temperature variation of the crossflow plate-fin heat exchanger plate wall (T_w) in the element is approximated by a four-noded quadrilateral in terms of local co-ordinates s and t, as,

$$T_w=N_iT_i+N_jT_j+N_kT_k+N_lT_l \quad (21)$$

where N_i, N_j, N_k and N_l and T_i, T_j, T_k and T_l are the shape functions and temperatures, respectively, for nodes i, j, k and l, and

$$N_i=1-\frac{s}{2b}-\frac{t}{2a}+\frac{st}{4ab} \quad N_j=\frac{s}{2b}-\frac{st}{4ab}$$

$$N_k=\frac{st}{4ab} \quad N_l=\frac{t}{2a}-\frac{st}{4ab}$$

where $2a=L$ and $2b=l$ ($L=l$ for square elements).

The following dimensionless parameters are introduced to study the influence of LHC on the exchanger performance:

- LHC parameter on the hot side (λ_h)

$$=[(kA_w)/LC]_h; \quad (22)$$

- LHC parameter on the cold side (λ_c)

$$=[kA_w)/LC]_c; \quad (23)$$

- conduction effect factor (τ) $=\varepsilon_{NC}-\varepsilon_{WC}/\varepsilon_{NC}$; (24)

where NC = no conduction and WC = with conduction.

The LHC effect factor (τ) directly shows the degree of deterioration of the exchanger effectiveness. Substituting the approximations in the above equations and using Galerkin's method [13], the final set of element matrices are obtained as shown in Appendix A for a crossflow plate-fin heat exchanger, Appendix B for counterflow/parallel-flow plate-fin heat exchangers and Appendix C for a crossflow tube-fin heat exchanger. In a crossflow plate-fin heat exchanger, the wall temperature distribution is two-dimensional. A four-noded element has been taken for wall temperature distribution. Hence, a 16×16 matrix has been obtained as shown in Appendix A for a crossflow plate-fin heat exchanger element. In the case of parallel-flow/counter-flow heat exchangers the wall temperature distribution is 1-D. A linear two-noted element has been taken for wall temperature distribution. Hence, a 10×10 matrix has been obtained as shown in Appendix B for a parallel-flow/counter-flow heat exchanger element. Similarly a 6×6 matrix has been obtained, considering 1-D temperature distribution in the tube, for a tube-fin heat exchanger as shown in Appendix C.

The element matrices for other pairs of the stacks in the strip are evaluated and assembled into a global matrix. The term Q_b is cancelled when the adjacent element is assembled. It only remains on the right-hand of the global matrix for the bottom pair of stacks. Similarly, the term Q_t remains only for the top pair of stacks. When the top and bottom surfaces are insulated, then Q_t and Q_b become zero. The final set of simultaneous equations are solved after incorporating the known boundary conditions (inlet temperatures).

For variable heat transfer coefficient cases, the marching technique is used, i.e. the outlet temperatures of strip 1 will be the inlet temperatures for adjacent strips. Thus by marching in a proper sequence, the temperature distribution in the exchanger is obtained. The element matrix for the case without LHC can be obtained when the temperature variation in the plates and tubes is neglected. Thus a seven-noded element matrix [10, 11] for a plate-fin exchanger and a five-noded element matrix for a tube-fin heat exchanger are obtained for the case without LHC. The heat transfer coefficients are evaluated at the bulk mean temperatures of the fluids. If the temperatures are not known *a priori*, the iteration is started with assumed outlet temperatures. The new outlet temperatures are calculated and compared with assumed outlet temperatures. The iterations are continued until convergence is achieved to the fourth digit for all cases. Analytical solutions without considering the effects of LHC are obtained using the solution

procedure given by Kays and London [3] and others [14–17].

RANGES OF THE DESIGN AND OPERATING PARAMETERS

In this study, the ranges of the design and operating parameters of the exchanger are as follows:

- NTU is 1.0–50.0;
- C_h/C_c (i.e. C_{min}/C_{max}) is 0.2–1.0;
- $\lambda = 0.0$, 0.005, 0.00625, 0.01, 0.0125, 0.02, 0.025, 0.04, 0.05, 0.06, 0.08, 0.1, 0.12, 0.15, 0.16, 0.18, 0.2 and 0.4;
- $\lambda_h/\lambda_c = 1.0$–5.0;
- $(\vartheta ha)_h/(\vartheta ha)_c = 0.5$, 1.0 and 2.0.

STABILITY OF THE METHOD

The accuracy of the solution depends on the number of the elements used. Actually, the number of elements used is determined by a compromise between the accuracy desired and the time required by the computer. Use of a greater number of subdivisions can not only produce results of a higher accuracy but can also enhance the convergence. For example, as shown in Fig. 2(a), the predicted values approach the available analytical solution [9] for a counterflow heat exchanger, with a maximum deviation of about 0.2%, when the number of divisions are around 70 for the case of $C_h/C_c = 1.0$ at NTU = 10.0 and $\lambda = 0.02$. However, the above analysis has been checked by taking more numbers of elements in the fluid flow direction for higher NTUs. It was found that when 70 divisions were used for higher NTUs, although the results were accurate to the third digit they required more solving time by the computer. Thus, in this analysis around 70 divisions were used in the flow direction for most of the cases of the counterflow heat exchanger. Similarly, the present analysis results have been compared with available solutions for a crossflow plate-fin heat exchanger [2, 8], as shown in Fig. 2(b).

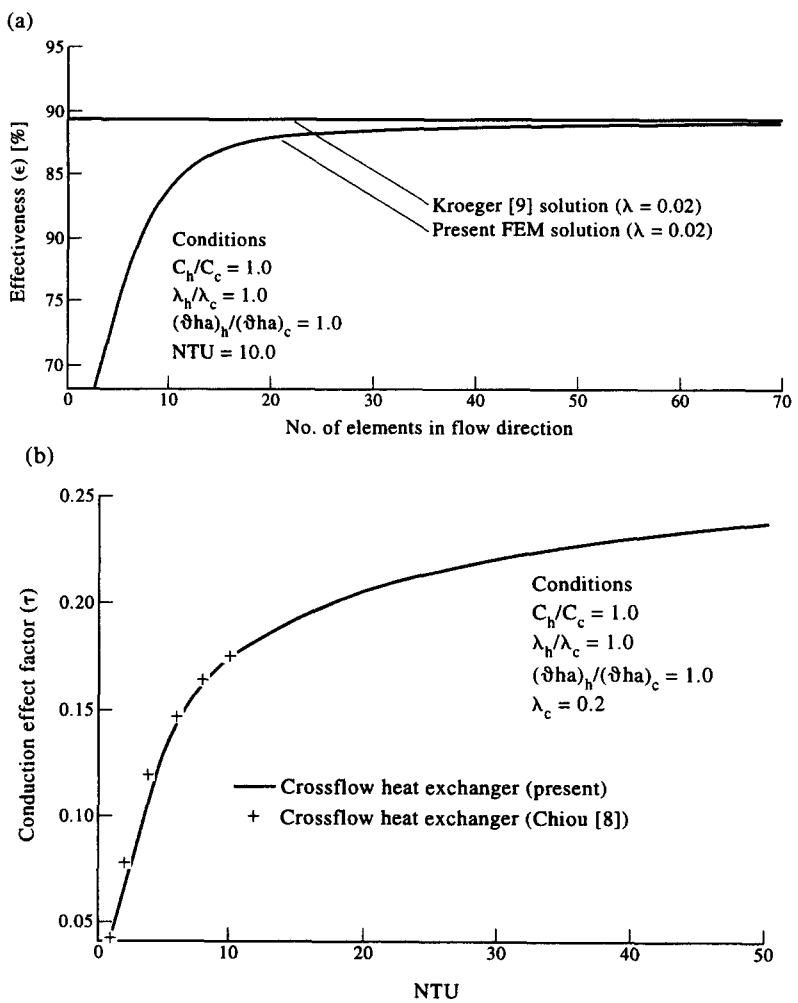

Fig. 2. LHC effects: (a) convergence of solution—counter-flow heat exchanger; (b) comparison of results with available solutions—crossflow plate-fin heat exchanger.

RESULTS AND DISCUSSION

In this analysis, 'air' is used as cold and hot fluids and the unmixed–unmixed type of exchangers is considered. In most cases, even a large variation in some physical properties will be reflected only marginally in the performance parameters as observed by other investigators [10, 11]. In this analysis, the heat exchanger surfaces (plain plate-fin surface—19.86 and strip-fin plate-fin surface—1/8–16.12(D)) which are obtained from Kays and London [3] are used for estimation of heat coefficients.

1. *Effects of LHC in crossflow heat exchanger*

In this paper, the performance evaluation with effects of LHC on a crossflow heat exchanger is presented, permitting predictions of conduction effects for balanced flow, $C_{min}/C_{max} = 1$, as well as for unbalanced flow, C_{min}/C_{max} not equal to one. However, the LHC effects for $C_h/C_c = 0.5$, 1.0 and 2.0 were available in the literature [2, 7, 8]. In order to contribute to the literature, the LHC effects have been extended to cases of $C_{min}/C_{max} = 0.8$, 0.6 and 0.4. The conduction effects are presented as a function of NTU ($NTU_{overall}$) and LHC parameter (λ) for three magnitudes of $C_{min}/C_{max} = 0.8$, 0.6 and 0.4, three magnitudes of $\lambda_h/\lambda_c = 0.5$, 1.0 and 2.0 and three magnitudes of $(\vartheta ha)_h/(\vartheta ha)_c = 0.5$, 1.0 and 2.0 in Fig. 3. These figures show that the conduction effect factor (τ) increases as λ increases for balanced as well-unbalanced flows, as shown by Chiou [7, 8]. In the case of unbalanced flow ($C_{min}/C_{max} = 0.8$) with higher λ (e.g. 0.2) values the conduction effect factor (τ) increases with NTU. However, in the case of unbalanced flows with lower λ values, the τ generally increases with NTU until NTU reaches approximately 6–10, and then it decreases with the increase of NTU, as shown in Fig. 3. Also, it has been observed that the τ increases with an increase of C_{min}/C_{max} values. For example, the maximum τ values (at NTU = 10, $\lambda = 0.2$ and $\lambda_h/\lambda_c = 1.0$) due to LHC effects are 0.175 for $C_{min}/C_{max} = 1$, 0.169 for $C_{min}/C_{max} = 0.8$, 0.138 for $C_{min}/C_{max} = 0.6$, and 0.093 for $C_{min}/C_{max} = 0.4$. These results are due to the exchanger unbalanced flow stream capacity rates which suppress the LHC effect, and are similar to those observed by other investigators and match with available numerical solutions [2, 7, 8].

The variations in performance deteriorations with $(\vartheta ha)_h/(\vartheta ha)_c$ ratio are presented in Fig. 3(d). These variations are smaller as observed by other investigators [2, 7, 8]. However, these results are presented to quantify the maximum error for $(\vartheta ha)_h/(\vartheta ha)_c = 0.5$ and 2.0 compared to $(\vartheta ha)_h/(\vartheta ha)_c = 1.0$ for various values of C_{min}/C_{max}. However, there are some significant variations in performance deteriorations due to LHC with λ_h/λ_c ratio and hence the present analysis has been carried out by considering the three magnitudes of $\lambda_h/\lambda_c = 0.5$, 1 and 2.0, as shown in Fig. 3.

2. *Effects of LHC in counterflow heat exchanger*

Closed-form analytical solutions are available [9] for LHC effects of counterflow heat exchangers. However, the LHC analysis has been conducted here for a counterflow heat exchanger to demonstrate the accuracy of FEM analysis. The FEM results of LHC effects for both balanced flow ($C_{min}/C_{max} = 1$) and unbalanced flow ($C_{min}/C_{max} = 0.6$) have been presented in Fig. 4, which are within 0.3% variation with closed-form analytical solutions [9].

It has been observed that the behaviour of performance deterioration due to LHC is similar to that of a crossflow heat exchanger, but the magnitudes of performance deteriorations are less when compared with a crossflow heat exchanger as shown in Fig. 4. For example, the maximum ineffectiveness values (at NTU = 10, $\lambda = 0.2$ and $\lambda_h/\lambda_c = 1$) are around 0.12 for $C_{min}/C_{max} = 1$ and 0.076 for $C_{min}/C_{max} = 0.6$.

3. *Effects of LHC in parallel-flow heat exchanger*

Also, in this paper, the performance deterioration due to LHC effects on a parallel-flow plate-fin heat exchanger are presented in Fig. 5 for both balanced ($C_{min}/C_{max} = 1$) and unbalanced ($C_{min}/C_{max} = 0.6$) flows. It has been observed that the performance deteriorations due to LHC are negligibly small. In this case, the wall temperature distribution is almost always flat regardless of the values of C_{min}/C_{max} and NTU. Since the temperature gradient in the wall is negligibly small in the fluid flow direction, the influence of LHC on the exchanger effectiveness is negligible. Hence, no study has been reported yet on the LHC problem for parallel-flow heat exchangers of either storage or direct transfer types. However, the present FEM analysis reveals that there are quantitative values of performance deteriorations due to LHC in a parallel-flow heat exchanger. The study shows that the performance deteriorations are negligibly small (less than 1%) when compared with counterflow and crossflow heat exchangers and may become insignificant as expected.

4. *Effects of LHC in crossflow tube-fin heat exchanger*

In crossflow tube-fin heat exchangers, the wall temperature distribution is one-dimensional and there is no analysis available yet for LHC effects. Hence, the FEM analysis has been extended to crossflow tube-fin heat exchangers; the results for both balanced flow ($C_{min}/C_{max} = 1$) and unbalanced flows ($C_{min}/C_{max} =$ 0.8, 0.6, 0.4 and 0.2) are presented in Fig. 6. It is interesting to note that for identical NTU and λ, the effect of LHC on the exchanger effectiveness is less for the crossflow tube-fin exchanger than for the crossflow plate-fin exchanger. Although this result is surprising, it is not unexpected since the temperature gradient in the tube in a crossflow tube-fin exchanger is linear and of lower magnitude compared to that in a crossflow plate-fin exchanger. Moreover, the shell-and-tube heat exchangers are usually designed for an exchanger effectiveness of 60% or below, per pass [2].

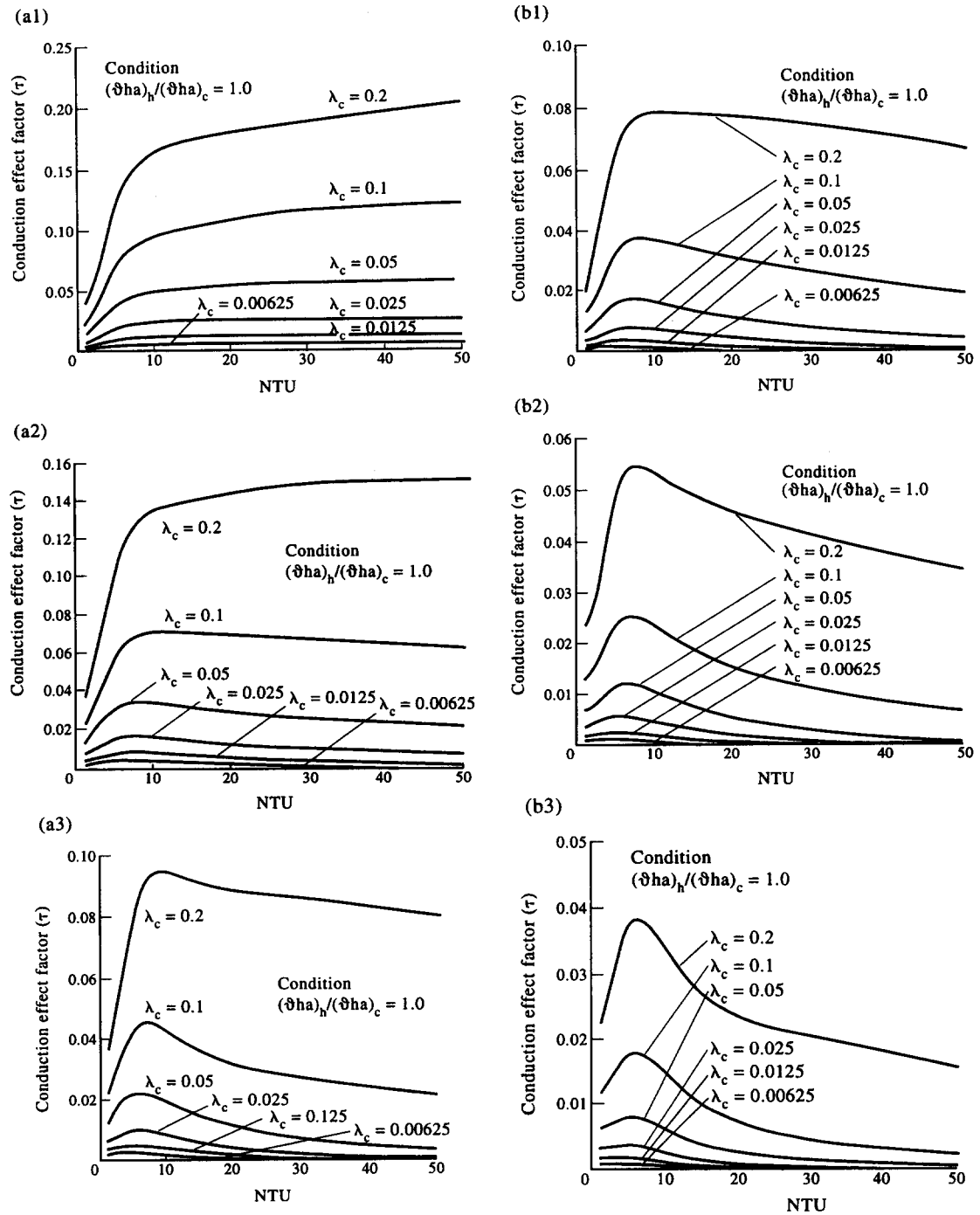

Fig. 3. LHC effects—crossflow plate-fin heat exchanger: (a1) $C_{min}/C_{max} = 0.8$ and $\lambda_h/\lambda_c = 1.0$; (a2) $C_{min}/C_{max} = 0.6$ and $\lambda_h/\lambda_c = 1.0$; (a3) $C_{min}/C_{max} = 0.4$ and $\lambda_h/\lambda_c = 1.0$; (b1) $C_{min}/C_{max} = 0.8$ and $\lambda_h/\lambda_c = 0.5$; (b2) $C_{min}/C_{max} = 0.6$ and $\lambda_h/\lambda_c = 0.5$; (b3) $C_{min}/C_{max} = 0.4$ and $\lambda_h/\lambda_c = 0.5$; (c1) $C_{min}/C_{max} = 0.8$ and $\lambda_h/\lambda_c = 2.0$; (c2) $C_{min}/C_{max} = 0.6$; and $\lambda_h/\lambda_c = 2.0$; (c3) $C_{min}/C_{max} = 0.4$ and $\lambda_h/\lambda_c = 2.0$; (d) conduction effects with $(\vartheta ha)_h/(\vartheta ha)_c$ ratio. (*Continued opposite.*)

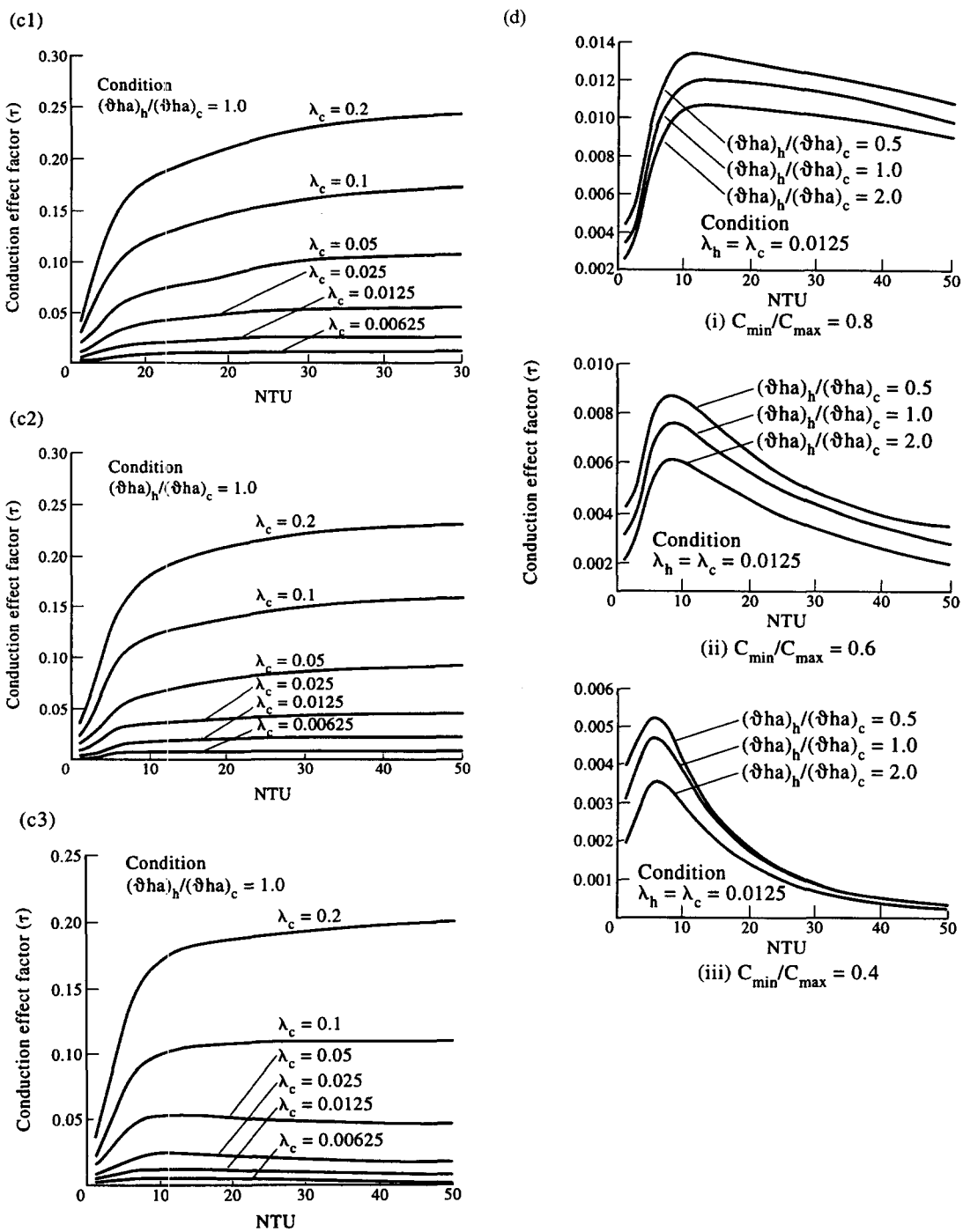

Fig. 3—*continued.*

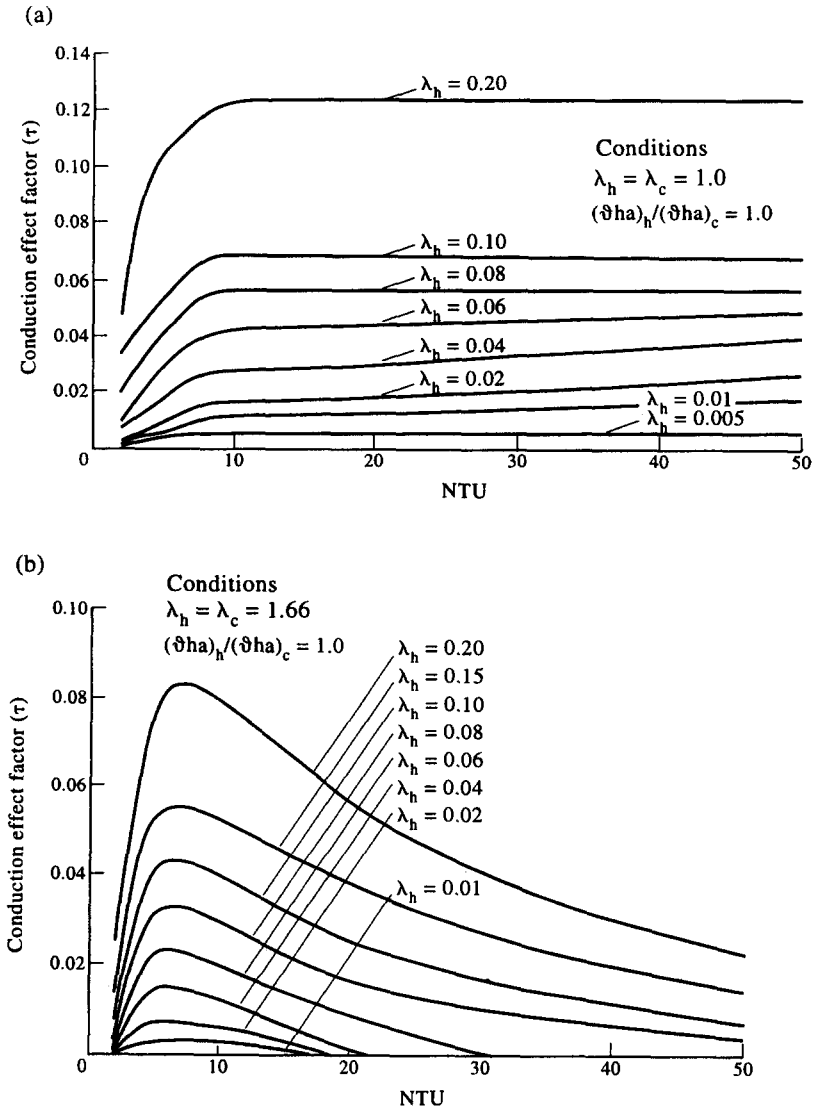

Fig. 4. LHC effects—counterflow heat exchanger: (a) $C_{min}/C_{max} = 1$; (b) $C_{min}/C_{max} = 0.6$.

In a tube-fin heat exchanger, the influence of heat conduction in the wall in the flow direction is negligible for low effectiveness values. The variations in performance deteriorations with $(\vartheta ha)_h/(\vartheta ha)_c$ ratio are smaller as shown in Fig. 6(f).

COMPARISON OF RESULTS—FOUR TYPES OF HEAT EXCHANGERS

The relations between the conduction effect factor (τ) and LHC parameters (λ) for a magnitude of C_{min}/C_{max} equal to 0.6 are compared in Fig. 7 for crossflow plate-fin, crossflow tube-fin counterflow plate-fin and parallel-flow plate-fin exchangers. It has been observed that the performance deteriorations of a crossflow plate-fin heat exchanger are higher than the counterflow and parallel-flow heat exchangers, for all cases. Also, it has been observed that the performance deteriorations of crossflow tube-fin heat exchangers are more or less equal to counterflow plate-fin heat exchangers. Although this result is surprising, it is not unexpected since the temperature gradient in the tube in a crossflow tube-fin exchanger is also linear. For the same NTU and C_{min}/C_{max}, the crossflow exchanger effectiveness is lower than the counterflow exchanger effectiveness, however, the wall temperature distribution is two-dimensional and results in higher temperature gradients for the crossflow exchanger. Since the crossflow exchangers are usually not designed for $\varepsilon > 80\%$, the LHC effect is generally small compared to a counterflow heat exchanger which is designed for ε up to 98–99%. Similarly, the shell-and-tube heat exchangers are usually not designed for $\varepsilon > 60\%$, so the LHC effect is gen-

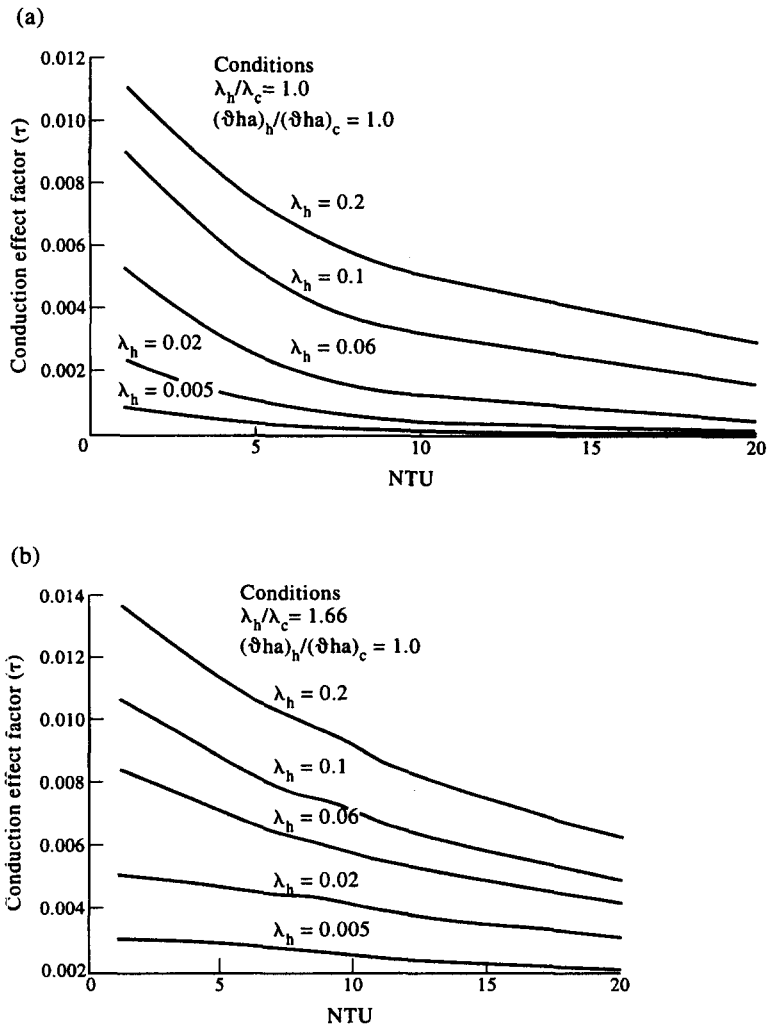

Fig. 5. LHC effects—parallel-flow heat exchanger: (a) $C_{min}/C_{max} = 1.0$; (b) $C_{min}/C_{max} = 0.6$.

erally small compared to a counterflow heat exchanger, or crossflow plate-fin heat exchanger.

CONCLUSIONS

The performance deteriorations of high-efficiency crossflow plate-fin, crossflow tube-fin counterflow plate-fin and parallel-flow plate-fin compact heat exchangers have been reviewed with effects of LHC on exchanger walls and tubes. Under the basic assumptions of constant material properties, and of no heat exchange between the exchanger and its environment, the performance deteriorations due to LHC on exchanger walls and tubes have been presented and evaluated for both balanced and unbalanced flows of crossflow plate-fin, crossflow tube-fin, counterflow plate-fin and parallel-flow plate-fin heat exchangers. The finite element model, introduced in this paper for the simple crossflow, counterflow and parallel-flow type heat exchangers, predicts thermal performance deteriorations which are within 0.1% variation with available analytical/numerical/approximate solutions.

The thermal performance deterioration of crossflow and counterflow compact heat exchangers due to LHC is not always negligible, especially when the capacity rate ratio of both fluids is equal to 1.0 and when the LHC parameter (λ) is greater than 0.005. Also, it was observed that the performance deteriorations of crossflow heat exchangers (especially crossflow plate-fin heat exchangers) are higher than the counterflow and parallel-flow heat exchangers for all cases because the wall temperature distribution is two-dimensional. Information obtained in this study clearly indicates that the deterioration of thermal performance due to LHC on exchanger walls and tubes, may be significant for crossflow and counterflow heat exchangers, and will be insignificant for parallel-flow heat exchangers in some typical applications as analysed in this paper.

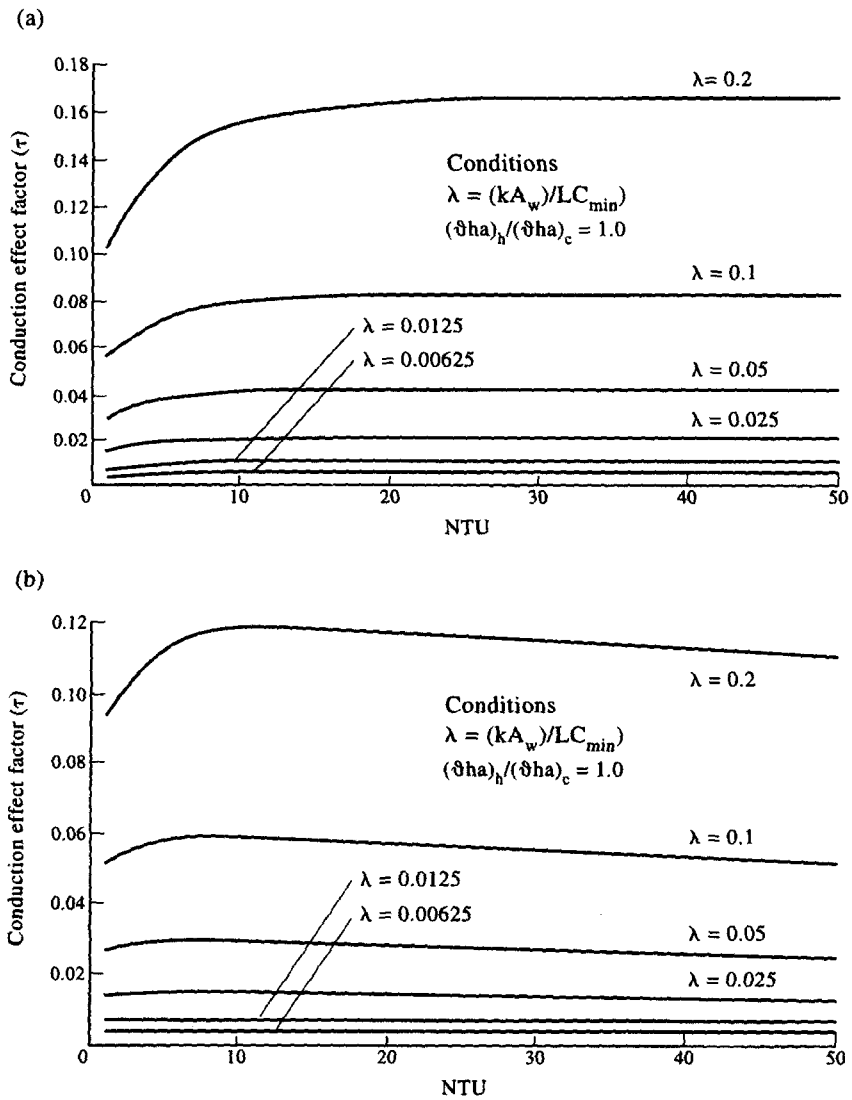

Fig. 6. LHC effects—crossflow tube-fin heat exchanger: (a) $C_{min}/C_{max} = 1.0$; (b) $C_{min}/C_{max} = 0.8$; (c) $C_{min}/C_{max} = 0.6$; (d) $C_{min}/C_{max} = 0.4$; (e) $C_{min}/C_{max} = 0.2$; (f) $C_{min}/C_{max} = 1.0$ with $(\vartheta ha)_h/(\vartheta ha)_c$ ratio.

(*Continued opposite and overleaf.*)

(c)

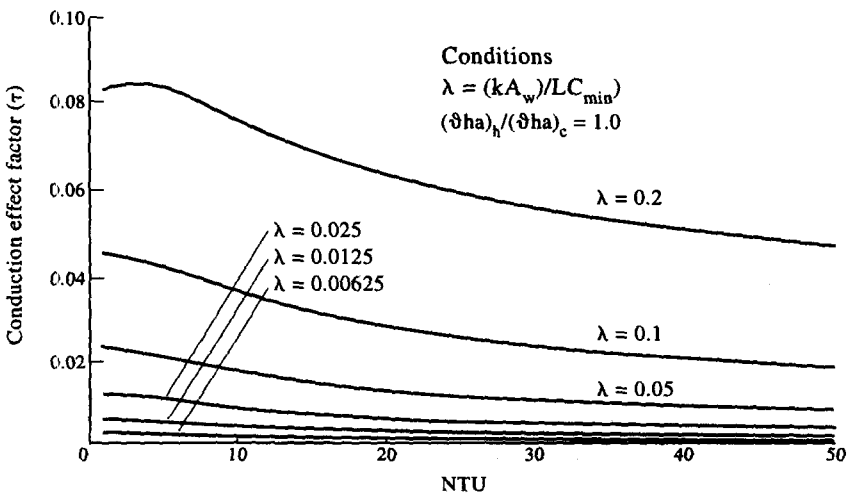

(d)

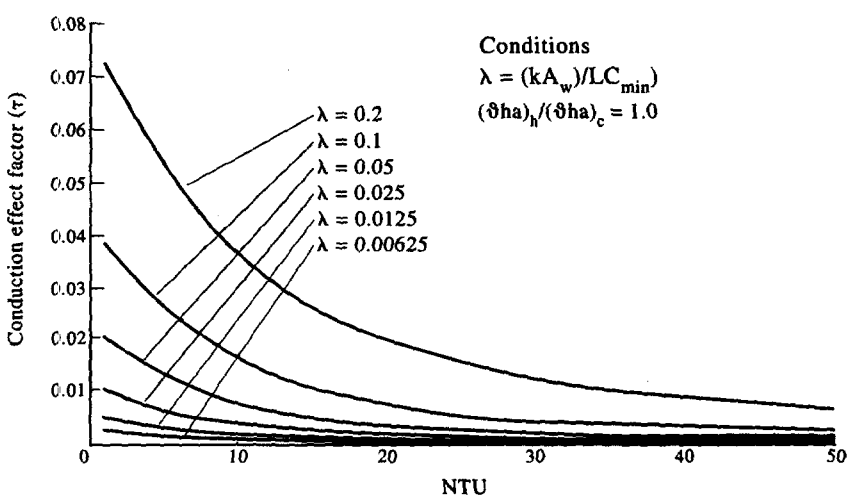

Fig. 6—*continued.*

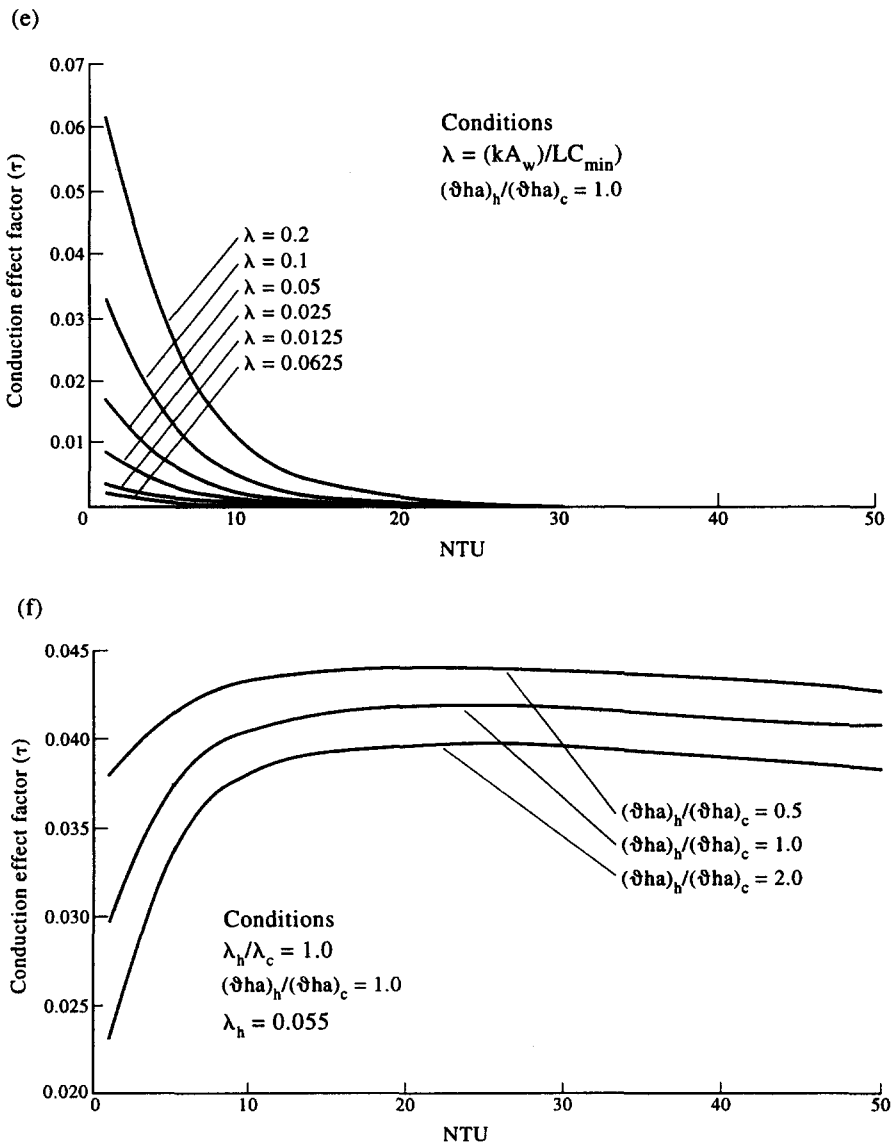

Fig. 6—*continued.*

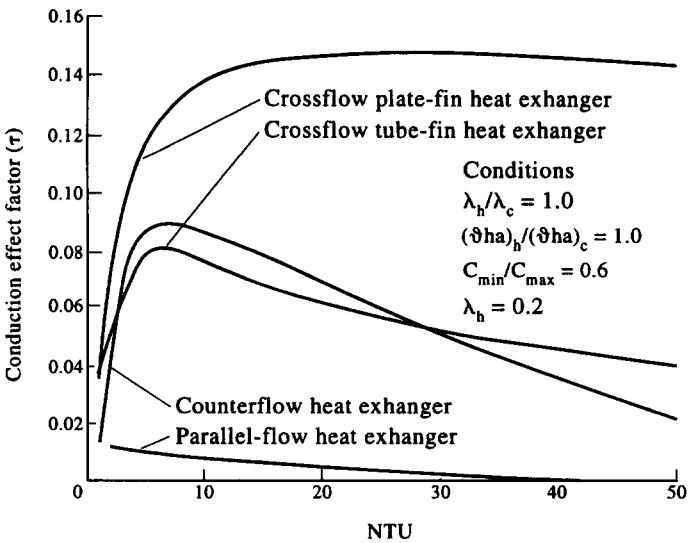

Fig. 7. LHC effects—comparison of four types of heat exchangers.

Acknowledgements—The authors are grateful to Dr R. K. Shah, Harrison Division, General Motors Corporation, New York, U.S.A. for his useful suggestions, during his visit to India, 1991, in carrying out this work. The authors wish to acknowledge their gratitude to the management of Hindustan Aeronautics Ltd, Bangalore-17, India for allowing publication of this paper.

REFERENCES

1. Holman, J. P., *Heat Transfer*, 4th edn, Chap. 10. McGraw-Hill, New York, 1981.
2. Shah, R. K., A review of longitudinal wall heat conduction in recuparators. *Journal of Energy, Heat and Mass Transfer*, 1994, **16**, 15–25.
3. Kays, W. M. and London, A. L., *Compact Heat Exchangers*, 3rd edn. McGraw-Hill, New York, 1984.
4. Bahnke, G. D. and Howard, C. P., The effect of longitudinal heat conduction on periodic-flow heat exchanger performance. *ASME Journal of Engineering for Power*, 1964, **86**, 121.
5. Shah, R. K., A correlation for longitudinal heat conduction effects in periodic-flow heat exchangers. *ASME Journal of Engineering for Power*, 1975, **97**, 453–454.
6. Shah, R. K., Counterflow rotary regenerator thermal design procedures. In *Heat Transfer Equipment Design*, ed. R. K. Shah, E. C. Subbarao and R. L. Mashelkar. Hemisphere, Washington, DC, 1988, pp. 267–296.
7. Chiou, J. P., The effect of longitudinal heat conduction on crossflow heat exchanger. *ASME Journal of Heat Transfer*, 1978, **100**, 346–351.
8. Chiou, J. P., The advancement of compact heat exchanger theory considering the effects of longitudinal heat conduction and flow nonuniformity effect. In *Compact Heat Exchangers—History, Technological Advancement and Mechanical Design Problems*, ed. R. K. Shah *et al.* ASME, New York, 1980, pp. 101–121.
9. Kroeger, P. G., Performance deterioration in high effectiveness heat exchangers due to axial heat conduction effects. *Advancements in Cryogenic Engineering*, 1966, **12**, 363–372.
10. Ravikurmar, S. G., Seetharamu, K. N. and Aswatha-Narayana, P. A., Performance evaluation of crossflow compact heat exchangers using finite elements. *International Journal of Heat and Mass Transfer*, 1989, **32**, 889–894.
11. Ravikumar, S. G., Seetharamu, K. N. and Aswatha-Narayana, P. A., Analysis of compact heat exchangers using finite element method. *Heat Transfer*, Vol. 2. Hemisphere, New York, 1986, pp. 379–384.
12. Chin, J. H. and Frank, D. R., Engineering finite element analysis of conduction, convection and radiation. In *Numerical Methods in Heat Transfer*, Vol. 3, ed. R. W. Lewis. Wiley, New York 1984.
13. Segerlind, L. J., *Applied Finite Element Analysis*, 2nd edn. Wiley, New York, 1982.
14. Yamasheta, H., Izumi, R. and Yamaguchi, S., Performance of crossflow heat exchangers with variable physical properties. *Bulletin of JSME*, 1977, **20**, 1008–1015.
15. Baclic, B. S., A simplified formula for crossflow heat exchanger effectiveness. *ASME Journal of Heat Transfer*, 1978, **100**, 746–747.
16. Baclic, B. S. and Heggs, P. J., On the search for new solutions of the single-pass crossflow heat exchanger problem. *International Journal of Heat and Mass Transfer*, 1985, **28**, 1965–1976.
17. Shah, R. K., Compact heat exchanger design procedures. In *Heat Exchangers: Thermal-Hydraulic Fundamentals and Design*, ed. S. Kakac, A. E. Bergles and F. Mayinger. Hemisphere, New York, 1981, pp. 111–151.

APPENDIX A

Crossflow plate-fin exchanger stack element matrix

$$
\begin{bmatrix}
C_1 & C_2 & C_3 & C_4 & -2K_2 & -K_2 & 0 & 0 & 0 & 0 & 0 & 0 & 0 & 0 & 0 & 0 \\
C_4 & C_5 & C_2 & C_6 & -K_2 & -K_2 & 0 & 0 & 0 & 0 & 0 & 0 & 0 & 0 & 0 & 0 \\
-2K_0 & -K_0 & 4K_0 & -K_0 & 0 & 0 & 0 & 0 & 0 & 0 & 0 & 0 & 0 & 0 & 0 & 0 \\
-K_0 & -2K_0 & -K_0 & 4K_0 & 0 & 0 & 0 & 0 & 0 & 0 & 0 & 0 & 0 & 0 & 0 & 0 \\
-2K_1 & -2K_1 & -K_1 & -K_1 & C_7 & C_8 & -K_1 & -K_1 & -K_1 & -K_1 & 0 & 0 & 0 & 0 & 0 & 0 \\
-K_1 & -K_1 & -2K_1 & -2K_1 & C_9 & C_{10} & -K_1 & -K_1 & -2K_1 & -2K_1 & 0 & 0 & 0 & 0 & 0 & 0 \\
0 & 0 & 0 & 0 & -2K_2 & -K_2 & C_{11} & C_{12} & C_{13} & C_{14} & -2K_6 & -K_6 & 0 & 0 & 0 & 0 \\
0 & 0 & 0 & 0 & -K_2 & -2K_2 & C_{14} & C_{15} & C_{12} & C_{16} & K_6 & 2K_6 & 0 & 0 & 0 & 0 \\
0 & 0 & 0 & 0 & 0 & 0 & -2K_4 & -K_4 & 4K_4 & -K_4 & 0 & 0 & 0 & 0 & 0 & 0 \\
0 & 0 & 0 & 0 & 0 & 0 & -K_4 & -2K_4 & -K_4 & 4K_4 & 0 & 0 & 0 & 0 & 0 & 0 \\
0 & 0 & 0 & 0 & 0 & 0 & -2K_5 & -2K_5 & -K_5 & -K_5 & C_{17} & C_{18} & -2K_5 & -2K_5 & -K_5 & -K_5 \\
0 & 0 & 0 & 0 & 0 & 0 & -K_5 & -K_5 & -2K_5 & -2K_5 & C_{19} & C_{20} & -K_5 & -K_5 & -2K_5 & -2K_5 \\
0 & 0 & 0 & 0 & 0 & 0 & 0 & 0 & 0 & 0 & -2K_6 & -K_6 & C_{21} & C_{22} & C_{23} & C_{24} \\
0 & 0 & 0 & 0 & 0 & 0 & 0 & 0 & 0 & 0 & -K_6 & -2K_6 & C_{24} & C_{25} & C_{22} & C_{26} \\
0 & 0 & 0 & 0 & 0 & 0 & 0 & 0 & 0 & 0 & 0 & 0 & -2K_8 & -K_8 & 4K_8 & -K_8 \\
0 & 0 & 0 & 0 & 0 & 0 & 0 & 0 & 0 & 0 & 0 & 0 & -K_8 & -2K_8 & -K_8 & 4K_8
\end{bmatrix}
\begin{bmatrix} T_1 \\ T_3 \\ T_3 \\ T_4 \\ T_5 \\ T_6 \\ T_7 \\ T_8 \\ T_9 \\ T_{10} \\ T_{11} \\ T_{12} \\ T_{13} \\ T_{14} \\ T_{15} \\ T_{16} \end{bmatrix}
=
\begin{bmatrix} 0 \\ 0 \\ 0 \\ 0 \\ 0 \\ 0 \\ 0 \\ 0 \\ 0 \\ 0 \\ 0 \\ 0 \\ 0 \\ 0 \\ 0 \\ 0 \end{bmatrix}
$$

where $K_0 = (kA_w)_t/6L$, $K_1 = (\vartheta ha)_h/12$, $K_2 = (\vartheta ha)_h/6$, $K_3 = (MC_p)/2$, $K_4 = (kA_w)_m/6L$, $K_5 = (\vartheta ha)_c/12$, $K_6 = (\vartheta ha)_c/6$, $K_7 = (MC_p)/2$, $K_8 = (kA_w)_b/6L$, $C_1 = 4k_0 + 2k_1$, $C_2 = 2K_1 - K_0$, $C_3 = K_1 - 2K_0$, $C_4 = K_1 - K_0$, $C_5 = 4K_0 + K_1$, $C_6 = -2K_0 + 2K_1$, $C_7 = K_3 + 4K_2$, $C_8 = 2K_2 - K_3$, $C_9 = 2K_2 + K_2$, $C_{10} = -K_3 + 4K_2$, $C_{11} = 4K_4 + 2K_1 + 2K_5$, $C_{12} = K_4 + 2K_1 + 2K_5$, $C_{13} = -2K_4 + K_1 + K_5$, $C_{14} = -K_4 + K_1 + K_5$, $C_{15} = 4K_4 + K_1 + K_5$, $C_{16} = -2K_4 + 2K_1 + 2K_5$, $C_{17} = K_7 + 4K_6$, $C_{18} = -K_7 + 2K_6$, $C_{19} = K_7 + 2K_6$, $C_{20} = -K_7 + 4K_6$, $C_{21} = 4K_8 + 2K_5$, $C_{22} = -K_8 + 2K_5$, $C_{23} = -2K_8 + K_5$, $C_{24} = -K_8 + K_5$, $C_{25} = 4K_8 + K_5$, and $C_{26} = -2K_8 + 2K_5$.

APPENDIX B

Counterflow/parallel-flow exchanger stack element

$$\begin{bmatrix} J1 & J2 & 2H & H & 0 & 0 & 0 & 0 & 0 & 0 \\ J2 & J1 & H & 2H & 0 & 0 & 0 & 0 & 0 & 0 \\ 2H & H & J3 & J4 & 2H & H & 0 & 0 & 0 & 0 \\ H & 2H & J5 & J6 & H & 2H & 0 & 0 & 0 & 0 \\ 0 & 0 & 2H & H & J7 & J8 & 2H & H & 0 & 0 \\ 0 & 0 & H & 2H & J8 & J7 & H & 2H & 0 & 0 \\ 0 & 0 & 0 & 0 & 2H & H & J3 & J4 & 2H & H \\ 0 & 0 & 0 & 0 & H & 2H & J5 & J6 & H & 2H \\ 0 & 0 & 0 & 0 & 0 & 0 & 2H & H & J1 & J2 \\ 0 & 0 & 0 & 0 & 0 & 0 & H & 2H & J2 & J1 \end{bmatrix} \begin{bmatrix} T_1 \\ T_2 \\ T_3 \\ T_4 \\ T_5 \\ T_6 \\ T_7 \\ T_8 \\ T_9 \\ T_{10} \end{bmatrix} = \begin{bmatrix} 0 \\ 0 \\ 0 \\ 0 \\ 0 \\ 0 \\ 0 \\ 0 \\ 0 \\ 0 \end{bmatrix}$$

where $K = kA_w/L$, $H = (9ha)/6$, $W = MC_p/2$, $J1 = K-2H$, $J2 = -K-H$, $J3 = W-4H$, $J4 = -W-2H$, $J5 = W-2H$, $J6 = -W-4H$, $J7 = K-4H$, and $J8 = -K-2H$.

APPENDIX C

Crossflow tube-fin exchanger stack element

$$\begin{bmatrix} -W_h+2H_h & W_h+H_h & -2H_h & -H_h & 0 & 0 \\ -W_h+H_h & W_h+2H_h & -H_h & -2H_h & 0 & 0 \\ -H_h & -H_h & K+H_h+2H_c & K+H_h+H_c & -2H_c & -H_c \\ -H_h & -2H_h & -K+H_h+H_c & K+2H_h+2H_c & -H_c & -2H_c \\ 0 & 0 & -2H_c & -H_c & -W_c+2H_c & W_c+H_c \\ 0 & 0 & -H_c & -2H_c & -W_c+H_c & W_c+2H_c \end{bmatrix} \begin{bmatrix} T_1 \\ T_2 \\ T_3 \\ T_4 \\ T_5 \\ T_6 \end{bmatrix} = \begin{bmatrix} 0 \\ 0 \\ 0 \\ 0 \\ 0 \\ 0 \end{bmatrix}$$

where $K = kA_w/L$, $H = (9hPL)/6$, $W = MC_p/2$.